# Vortex states in mesoscopic three-band superconductors

San Gillis,[1] Juha Jäykkä,[2] and Milorad V. Milošević[1]
[1]*Departement Fysica, Universiteit Antwerpen, Groenenborgerlaan 171, B-2020 Antwerpen, Belgium*
[2]*Nordita, KTH Royal Institute of Technology and Stockholm University Roslagtstullsbacken 23, SE-106 91 Stockholm, Sweden*
(Received 3 October 2013; revised manuscript received 5 December 2013; published 24 January 2014)

Using multicomponent Ginzburg-Landau simulations, we show a plethora of vortex states possible in mesoscopic three-band superconductors. We find that mesoscopic confinement stabilizes chiral states, with nontrivial phase differences between the band condensates, as the ground state of the system. As a consequence, we report the broken-symmetry vortex states, the chiral states where vortex cores in different band condensates do not coincide (split-core vortices), as well as fractional-flux vortex states with broken time-reversal symmetry.

DOI: 10.1103/PhysRevB.89.024512 PACS number(s): 74.25.Ha, 74.25.N−, 74.25.Uv

## I. INTRODUCTION

$MgB_2$ was discovered to be superconducting in 2001,[1] as a first two-gap superconductor, with the highest critical temperature $T_c = 39$ K of all binary compound metallic superconductors known today. Comparing with other known electron-phonon mediated superconductors, this $T_c$ is exceptionally high, and is thought to be due to the interaction between the two superconducting gaps and pairing anisotropy between the contributing electronic bands.[2] The gaps in $MgB_2$ have been experimentally measured using scanning tunneling spectroscopy,[3,4] point contact spectroscopy,[5,6] and heat capacity experiments.[7,8] Although multiband superconductors have been theoretically proposed over 50 years ago,[9,10] it was only after this discovery that there was renewed theoretical and experimental interest in multiband superconductivity.

Multiband superconductors can exhibit new phenomena not present in conventional single-band superconductors. Going back to $T_c$, one should mention the possibility of resonance (i.e., large enhancement of $T_c$) in cases when chemical potential is close to one of the bands.[11–13] Another new phenomenon that occurs in two- (and multi) band superconductors is the one of *hidden criticality*.[14] When two bands are weakly coupled, the coherence length of the weaker band shows a pronounced peak close to a hidden critical temperature, in stark contrast with the monotonic behavior of the coherence length as a function of temperature in single-band superconductors.[15] Such a phenomenon would be best visible in the behavior of vortex matter, which is also known to be rich in multiband superconductors. For example, theory predicts there is a possibility of vortex states with nonmonotonic intervortex interactions, namely short-range repulsion and long-range attraction due to competing length scales of different band condensates,[16–20] resulting in unusual vortex patterns.[21,22] Not only is the interaction between vortices markedly different from the single-band case, but it is also possible to stabilize fractional vortices in different band condensates of a multiband superconductor[23–25] (still with an integer total magnetic flux in units of flux quanta).

Related to length scales, it is well known that confined superconductivity on the mesoscopic scale brings forth interesting behavior, such as enhancement of critical magnetic field[26,27] or the Little-Parks effect.[28,29] Additionally, the boundary can impose its symmetry on the vortex matter, enabling, e.g., formation of giant vortices.[26,30–35] For two-gap superconductors it was shown that noncomposite and fractional vortex states can be thermodynamically stabilized by the mesoscopic boundary[36–42] due to the different interaction of two-band condensates with the mesoscopic confinement.

The recent discovery of iron-based superconductors[43–45] has further increased interest in multiband superconductors, since these materials typically have more than two coupled superconducting bands[46,47] (e.g., exactly three contributing bands have been recently identified in LiFeAs[48]). The interband scattering (i.e., coupling between bands) can then impose a specific phase difference between the different components of the superconducting order parameter. This allows inherently new physics not present in single-band or two-band superconductors, due to frustration between the phase locking tendencies, leading to states with spontaneously broken time-reversal symmetry (BTRS).[49–53] Generally speaking, this frequently called *chiral* state brings forward a plethora of unexplored physics, which can be imagined via analogy with a Josephson effect but between several bands in the $k$ space, with different (though related) phase shifts between different bands. For the same reason, one of the possible smoking guns for chiral superconductivity are specific properties of real Josephson junctions made of chiral superconductors (see Ref. 54).

Another smoking gun for the underlying physics in three-band superconductors is the vortex matter, being relatively easily observable in experiment. In Refs. 49 and 50 the topological solitons with broken time-reversal symmetry, essentially chains of fractional vortices, were predicted stable in bulk chiral samples. In this paper we study the influence of the mesoscopic confinement on the BTRS vortex states. We look at a system with one strong superconducting band, which couples to two other bands which are only superconducting due to the interaction with the first band (the usual situation for temperatures close to $T_c$). The coupling between bands is of the form $(++-)$, meaning that the order parameters of second and third band prefer to have a phase difference of $\pi$ while trying to attain the same phase as the first band. It is clear that this can lead to frustration, and nontrivial phase differences between the bands. As we will show, such chiral superconducting state is indeed stable, and becomes the ground

 

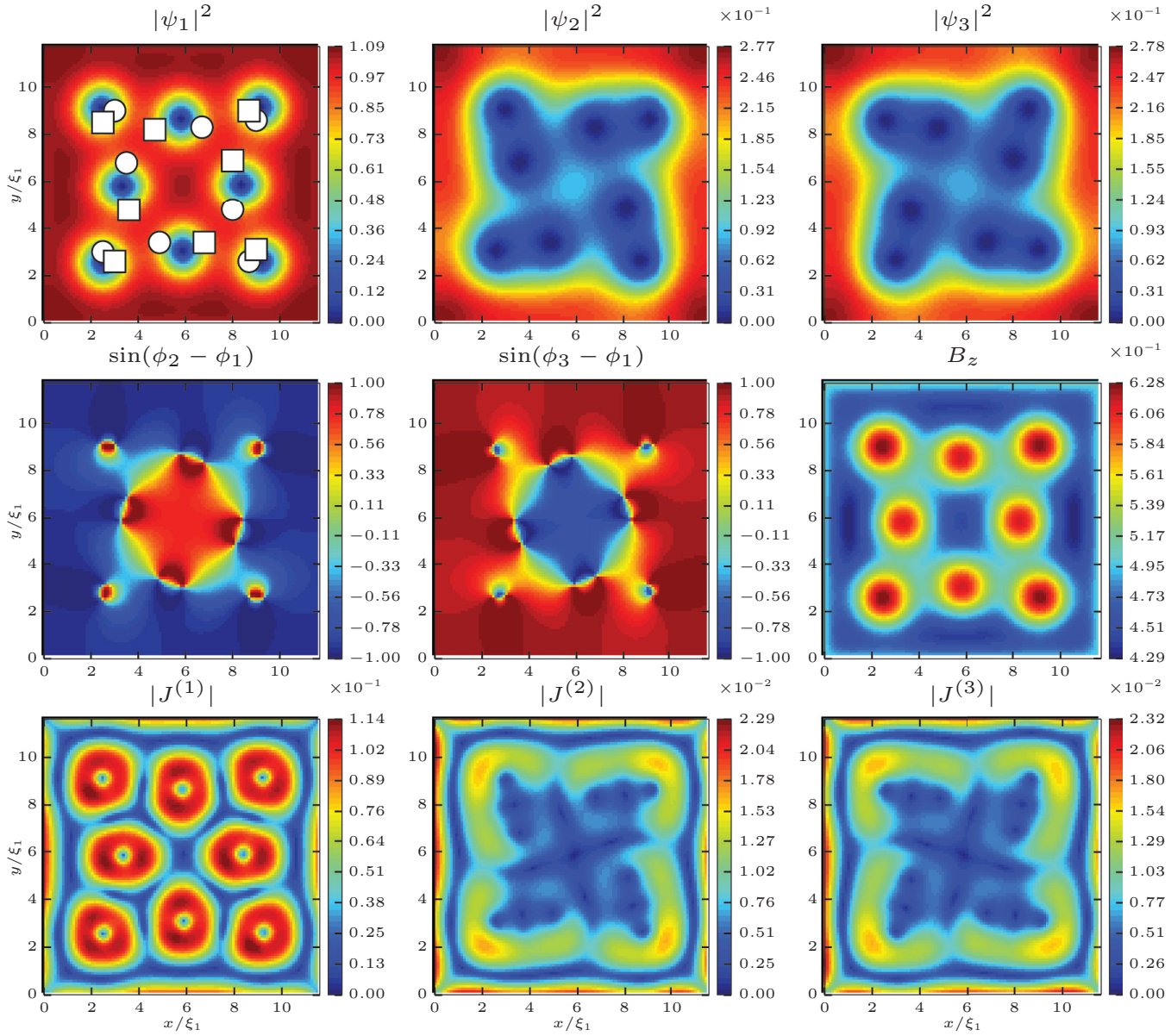


FIG. 1. (Color online) One of the four initial states used in the simulations, created by shrinking the known ($N = 8$, see Ref. 49) soliton solution for bulk three-band superconductors to a mesoscopic size. Different panels show: The Cooper-pair density of different band condensates ($\psi_{i=1,2,3}$), the phase difference between the bands, spatial distribution of the total magnetic field $B_z$, and magnitude of the three components to the current ($J_{i=1,2,3}$), each stemming from a different band condensate. In the Cooper-pair density plot for the first condensate (top-left panel), the locations of vortices in the second and the third condensate are shown by white dots and squares, respectively.

state in mesoscopic samples. Moreover, the mesoscopic boundary interacts with the phase domain walls in the sample. Those domain walls energetically favor splitting of vortex lines in different bands, and their interaction with mesoscopic boundary enables a plethora of possible states unattainable in bulk or nonchiral mesoscopic samples—including chiral fractional vortices, where vorticity is not equal in all band condensates in addition to broken time-reversal symmetry. We finally offer a classification of the observed vortex states, richer than ones found in any other superconducting system studied to date. Our findings are particularly important in the context of the recent progress in growth, fabrication, and nanopatterning of single-crystal and thin-film multiband superconductors, iron-based[55] or otherwise (e.g., doped fullerides,[56] ruthanates,[57] or nanothin films of elementary superconductors[58–60]).

The paper is organized as follows. In Sec. II we introduce the Ginzburg-Landau model for three-component superconductors. We express the Ginzburg-Landau coefficients in the microscopic framework to facilitate comparison with experiment. In Sec. III we discuss the observed vortex states and order them in three main classes, with several subdivisions. Our summary and conclusions are given in Sec. IV.

## II. THEORETICAL FORMALISM

In this paper we perform theoretical simulations in the framework of the three-component Ginzburg-Landau model.

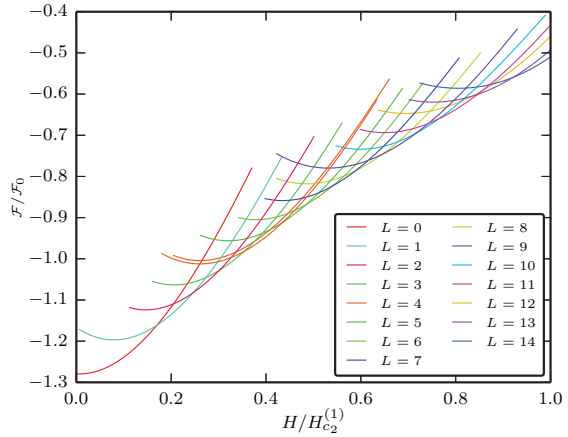


FIG. 2. (Color online) Energy of all found conventional (composite, not fractional, not chiral) vortex states as a function of the applied external magnetic field. $L$ denotes the vorticity of the state.

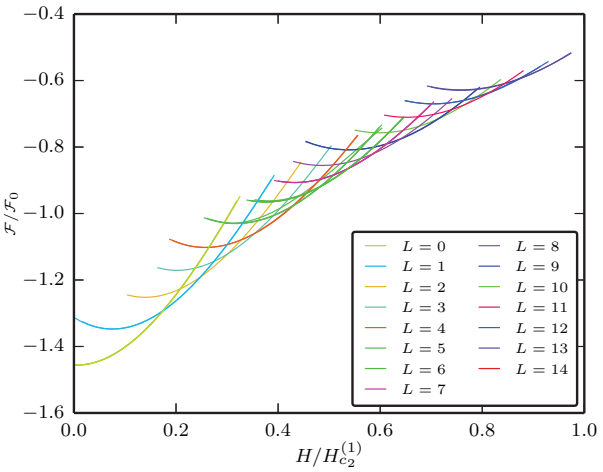


FIG. 4. (Color online) Energy of all found chiral composite vortex states as a function of the applied external magnetic field.

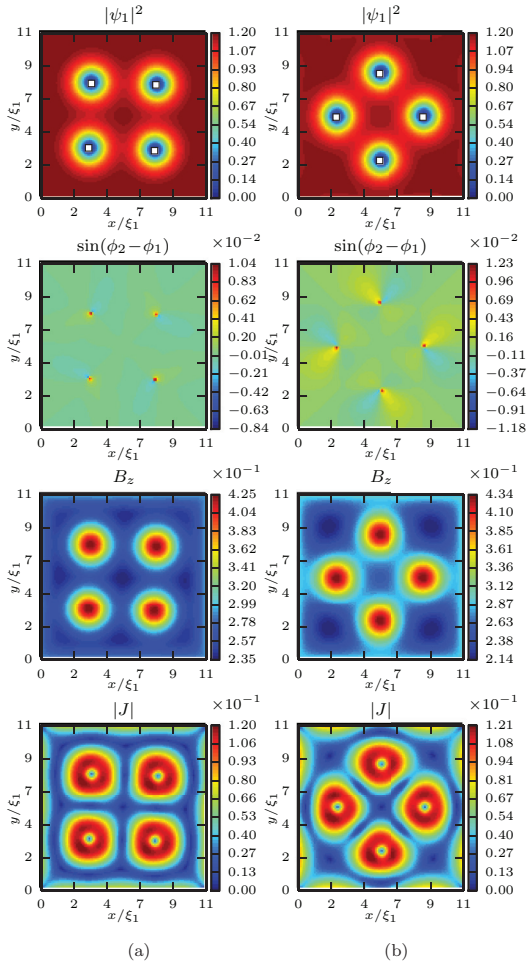


FIG. 3. (Color online) Conventional vortex state with vorticity $L = 4$ in all bands (a), and an alternative higher energy state (b). Panels (top to bottom) show the Cooper-pair density of the first band with superimposed locations of vortices in other bands, the phase difference between the band condensates 1 and 2, the distribution of the magnetic field, and total current in the sample.

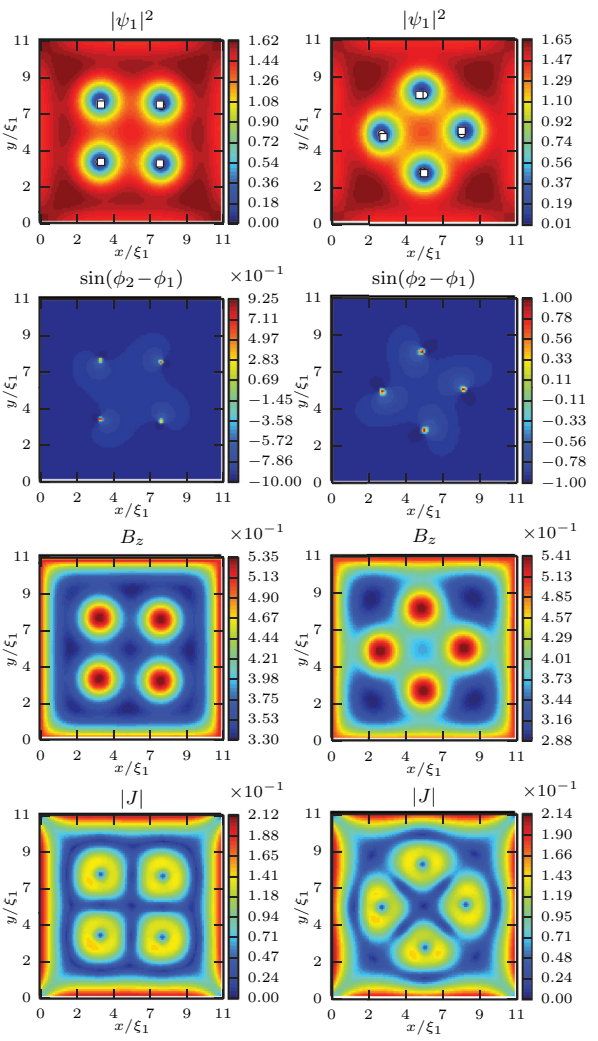


FIG. 5. (Color online) Two found configurations of four vortices in a chiral vortex state, presented in the same manner as Fig. 3.

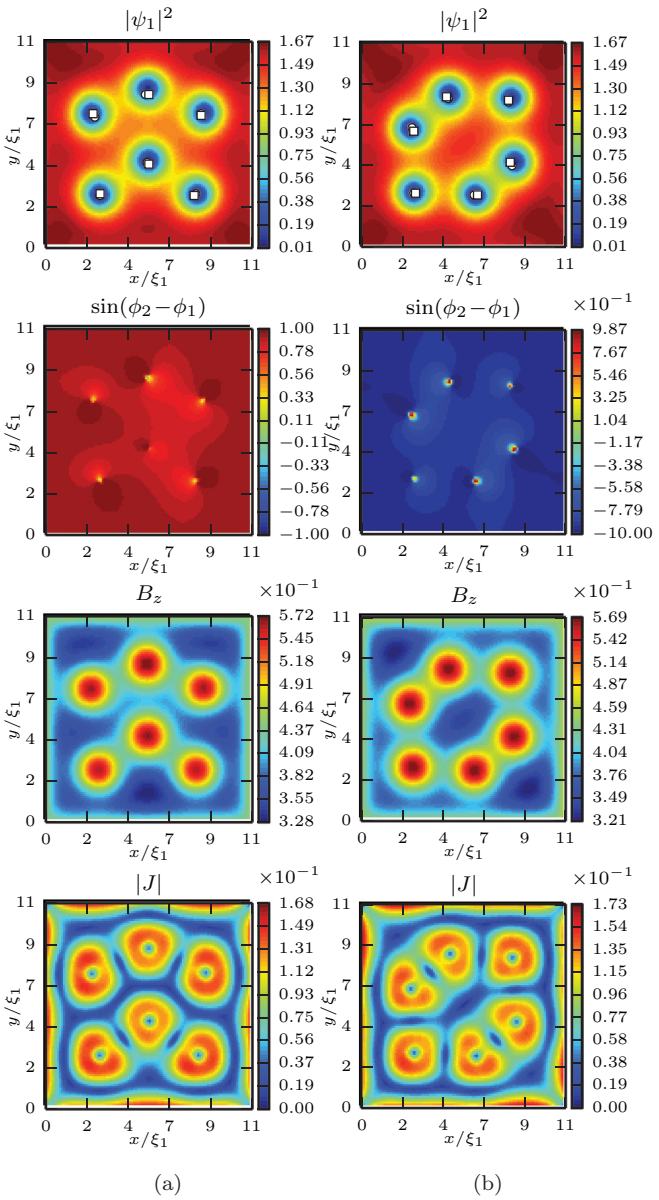


FIG. 6. (Color online) Two found configurations of six vortices in a chiral vortex state, presented in the same manner as Fig. 5.

The governing energy functional takes the form

$$\mathcal{F} = \int dV \left[ \sum_{i=1}^{3} \left( \alpha_i |\Psi_i|^2 + \frac{1}{2}\beta_i |\Psi_i|^4 \right) - \sum_{i=0}^{3} \sum_{j>i}^{3} \eta_{ij} |\Psi_i||\Psi_j| \cos(\phi_i - \phi_j) + \sum_{i=1}^{3} \frac{1}{2m_i} \left| \left( -i\hbar\nabla - \frac{2e}{c}\vec{A} \right) \Psi_i \right|^2 + \frac{(\nabla \times \vec{A})^2}{8\pi} \right], \tag{1}$$

where $\mathcal{F}$ is the difference in free energy between the superconducting and normal state, $\Psi_i$ are the complex order parameters of the band condensates (with phase $\phi_i$), $\vec{A}$ is the vector potential, $\alpha_i$, $\beta_i$ are the phenomenological GL coefficients, $\eta_{ij}$ denote the "Josephson" couplings between the bands, and $i$ and $j$ are the band indices.

We next rewrite Eq. (1) in a dimensionless form by scaling length to units of $\xi_1 = \hbar/\sqrt{-2m_1\alpha_1}$, the order parameters to $\Psi_{10} = -\alpha_1/\beta_1$, the vector potential to $A_0 = \hbar c/2e\xi_1$ (thus magnetic field is scaled to $H_{c_2}^{(1)} = \hbar c/2e\xi_1^2$), and free energy to $\mathcal{F}_0 = \xi_1^3\alpha_1^2 V/\beta_1$, where $V$ is the volume of the sample. The dimensionless energy functional reads

$$\frac{\mathcal{F}}{\mathcal{F}_0} = \frac{1}{V}\int dV \left[ \sum_{i=1}^{3} \left( \frac{\alpha_i}{|\alpha_1|}|\Psi_i|^2 + \frac{1}{2}\frac{\beta_i}{\beta_1}|\Psi_i|^4 \right) - \sum_{i=0}^{3}\sum_{j>i}^{3} \frac{\eta_{ij}}{|\alpha_1|}|\Psi_i||\Psi_j|\cos(\phi_i - \phi_j) + \sum_{i=1}^{3} \frac{m_1}{m_i}|(\nabla - i\vec{A})\Psi_i|^2 + \kappa_1^2(\nabla \times \vec{A})^2 \right], \tag{2}$$

where $\kappa_1 = (H_{c_2}^{(1)})^2\xi_1^3/8\pi\mathcal{F}_0 V$. The free energy is then minimized numerically in order to obtain solutions to the GL model. The fields found from this minimization will automatically be solutions to the equations of motion:

$$\frac{\alpha_i}{|\alpha_1|}\psi_i + \frac{\beta_i}{\beta_1}|\psi_i|^2\psi_i - \sum_{j\neq i}\frac{\eta_{ij}}{|\alpha_1|}\psi_j + \frac{m_1}{m_i}(\nabla - i\vec{A})^2\psi_i = 0, \tag{3}$$

$$\vec{J} = \sum_{i=1}^{3}\vec{J}_i = \nabla \times \nabla \times \vec{A} = \sum_{i=1}^{3}\frac{m_1}{2m_i\kappa_1^2}[i\left(\bar{\psi}_i\nabla\psi_i - \psi_i\nabla\bar{\psi}_i\right) + |\psi_i|^2\vec{A}]. \tag{4}$$

To closer relate our results to known superconducting materials, we express the GL coefficients in terms of microscopic parameters, following Ref. 52, as

$$\alpha_i = N(0)\gamma_{ii} - N_i(0)\mathcal{A} - N_i(0)\tau, \tag{5}$$

$$\beta_i = N_i(0)\frac{7\zeta(3)}{8\pi^2 T_c}, \tag{6}$$

$$\mathcal{K}_i = \frac{\hbar^2}{2m_i} = \xi_i^2|\alpha_i| = \frac{\beta_i}{6}\hbar^2 v_i^2, \tag{7}$$

$$\eta_{ij} = N(0)\gamma_{ij}, \tag{8}$$

where $N(0) = \sum_{i=1}^{3} N_i(0)$ is the total density of states, $\mathcal{A} = \ln[(2e^{\Gamma}\hbar\omega_D)/(\pi T_c)]$ with $\Gamma$ the Euler constant and $\omega_D$ the Debye energy, and $\tau = \ln(T/T_c)$. $v_i$ are the band dependent Fermi velocities, and $\gamma_{ij}$ denote the elements of the inverted interaction matrix.

Considering that microscopic parameters of relevant materials are not yet known with certainty, in what follows we will choose a set of Ginzburg-Landau parameters, and just note that it is possible to integrate real microscopic parameters in

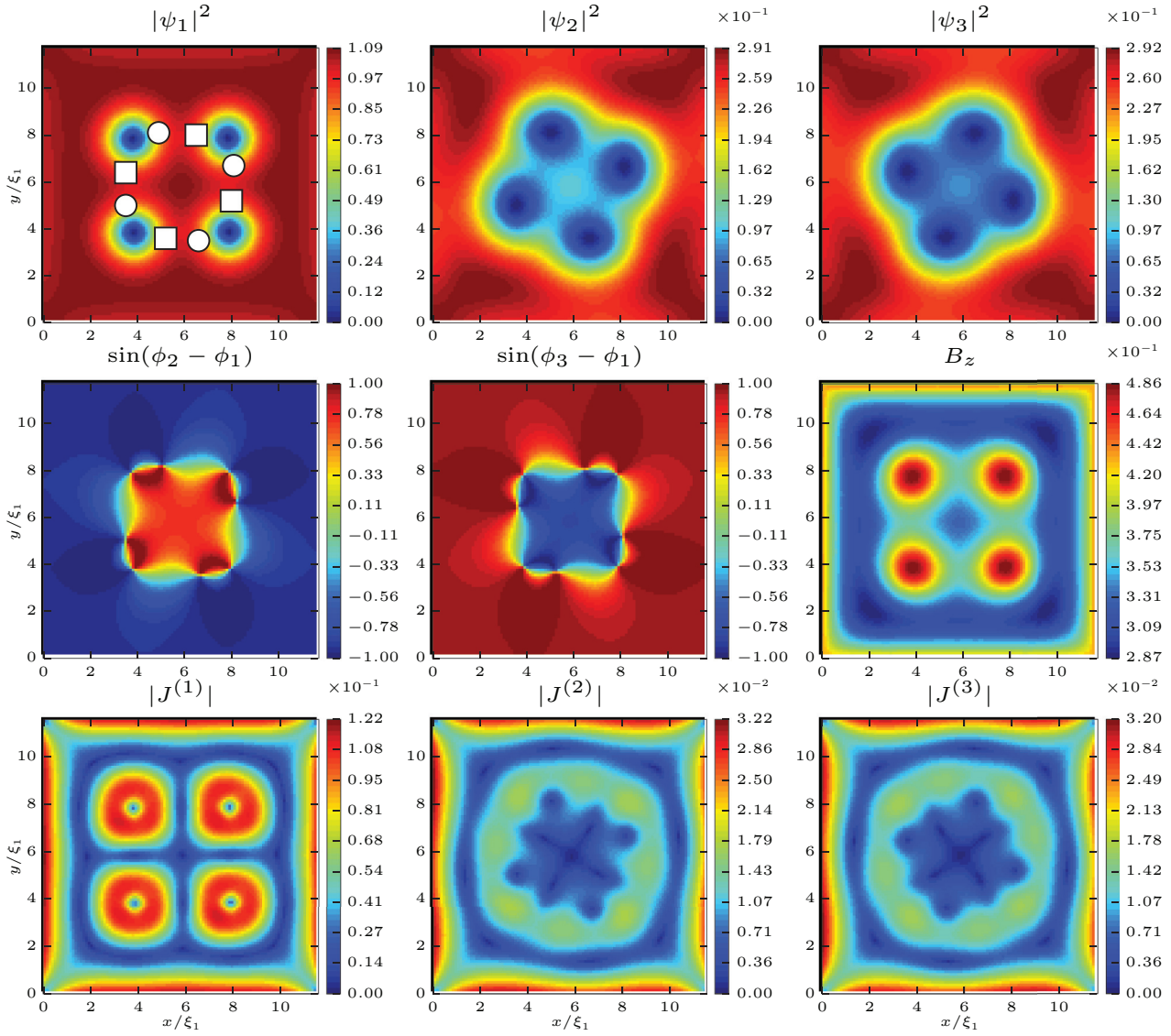


FIG. 7. (Color online) Chiral $L = 4$ vortex state with an internal phase domain wall, illustrated in the same format as Fig. 1.

the study:

$$\frac{\alpha_i}{|\alpha_1|} = \left(-1, \frac{2}{3}, \frac{2}{3}\right), \quad \frac{\beta_i}{\beta_1} = (1,1,1),$$
$$\frac{\eta_{ij}}{|\alpha_1|} = \left(\frac{2}{3}, \frac{2}{3}, -2\right), \quad \frac{m_1}{m_i} = (1,1,1).$$

With this choice of parameters, we consider three bands with same parameters except for the elements in the interaction matrix, i.e., only the coupling constants between the bands will differ, as well as the respective critical temperatures of the bands. Such a choice will enable us to more easily differentiate the effects of chirality from the other forms of competition between the band condensates.

In the numerical approach we search for as many solutions as possible to the equations of motion Eqs. (3) and (4). We do this by starting from four different initial configurations: (i) The Meissner state with no phase difference between the condensates, (ii) the Meissner state with phase difference between the condensates, (iii) a field-cooled condition, i.e.,

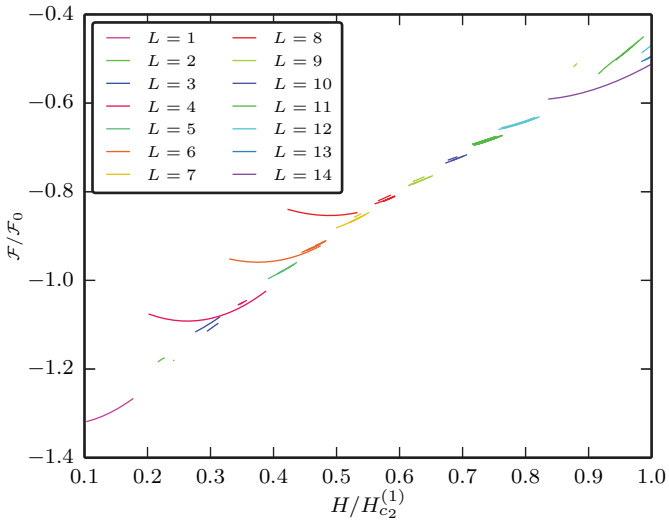


FIG. 8. (Color online) Energy curves of the found chiral vortex states with phase domain walls, and consequently split-core vortices.

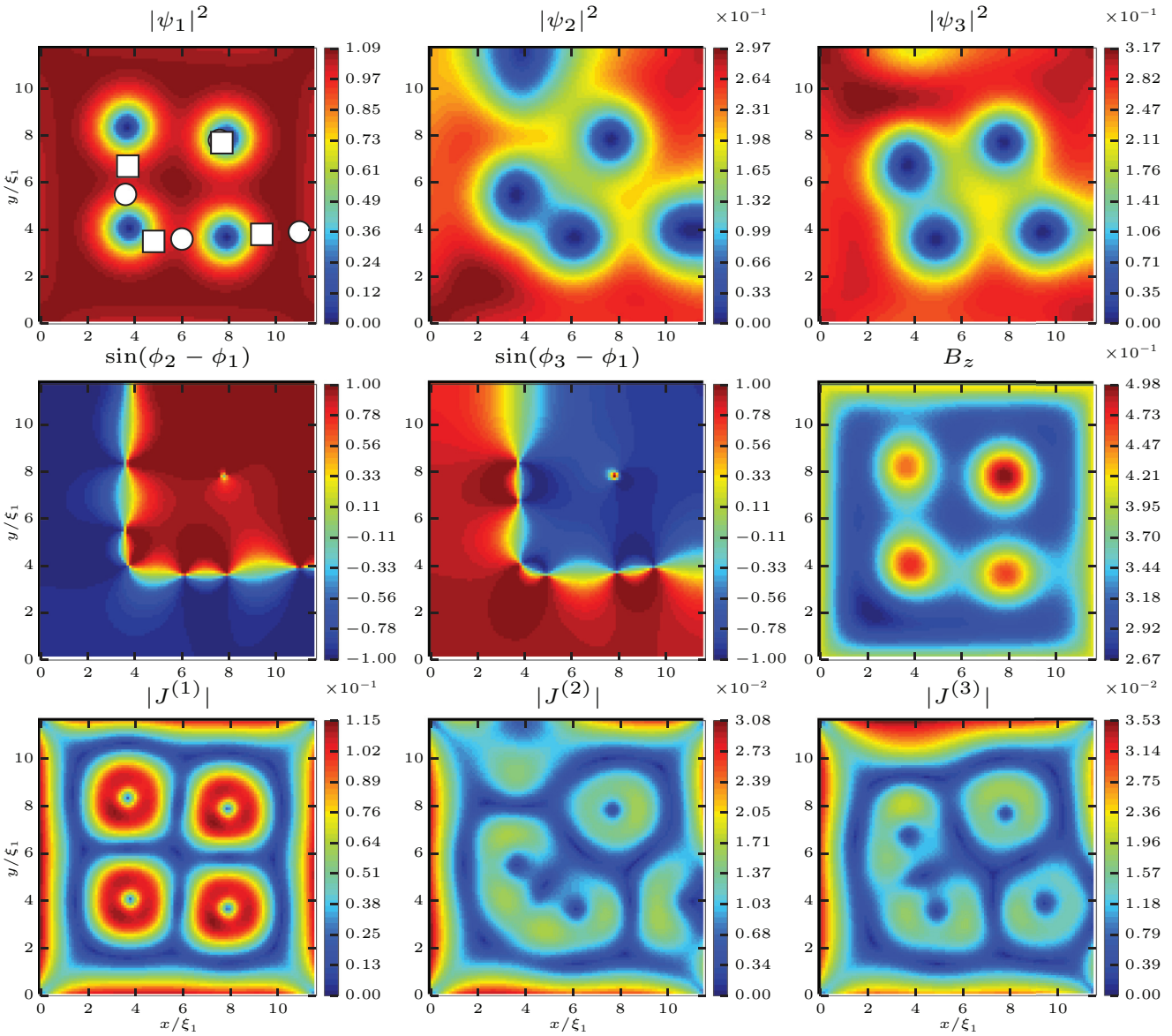


FIG. 9. (Color online) Chiral $L = 4$ vortex state with a phase domain wall connecting adjacent sides of the sample, illustrated in the same format as Fig. 7 for facilitated comparison of all relevant quantities.

weak and fluctuating order parameter in each band, and (iv) a state found by recreating the $N = 8$ soliton solution from Ref. 49 and shrinking this state to a size of $12\xi_1$ by $12\xi_1$. The exemplary result of the latter operation is shown in Fig. 1. From each of the initial states, we sweep the external magnetic field up and down. At certain values of the magnetic field, the system will jump to a new state with different vorticity. These states are saved, and from each new state, we do a new sweep of the magnetic field in both directions to uncover other possible states.

As a final comment regarding sample description, we will present the data obtained for a square sample of size $12\xi_1$ by $12\xi_1$, but we have performed calculations and found qualitatively the same results for samples of size up to $40\xi_1$ by $40\xi_1$ [corresponding to samples of known three-band materials (e.g., iron-based ones) of approximately 0.5 $\mu$m by 0.5 $\mu$m in size, closer to $T_c$]. This indicates that our conclusions about found vortex states are not restricted to strongly confined systems, and can also be relevant to much larger systems (i.e., vortex phenomenology close to the sample boundaries).

Lastly, we describe the details of the numerical procedure, regarding discretization and numerical implementation of the energy minimization. At every value of the magnetic field in a sweep, we re-relax the free energy in order to find a solution to the equations of motion at that magnetic field. We do this by using the standard link-variable discretization scheme with one-point forward differences to discretize the energy functional $\mathcal{F}$ on a square lattice of spacing $h$. The lattice is subdivided into $N_i \times N_j$ points, and $N_i = N_j = 120$ in all simulations reported in this paper. This discretization has been used before in Ref. 25, however it is now extended to include an arbitrary number of complex order parameters and the corresponding Josephson couplings. The applied magnetic field $\mathbf{B}$ is implemented by giving $\mathbf{A}$ a boundary condition such that $\nabla \times \mathbf{A} = \mathbf{B}$ on the boundary.

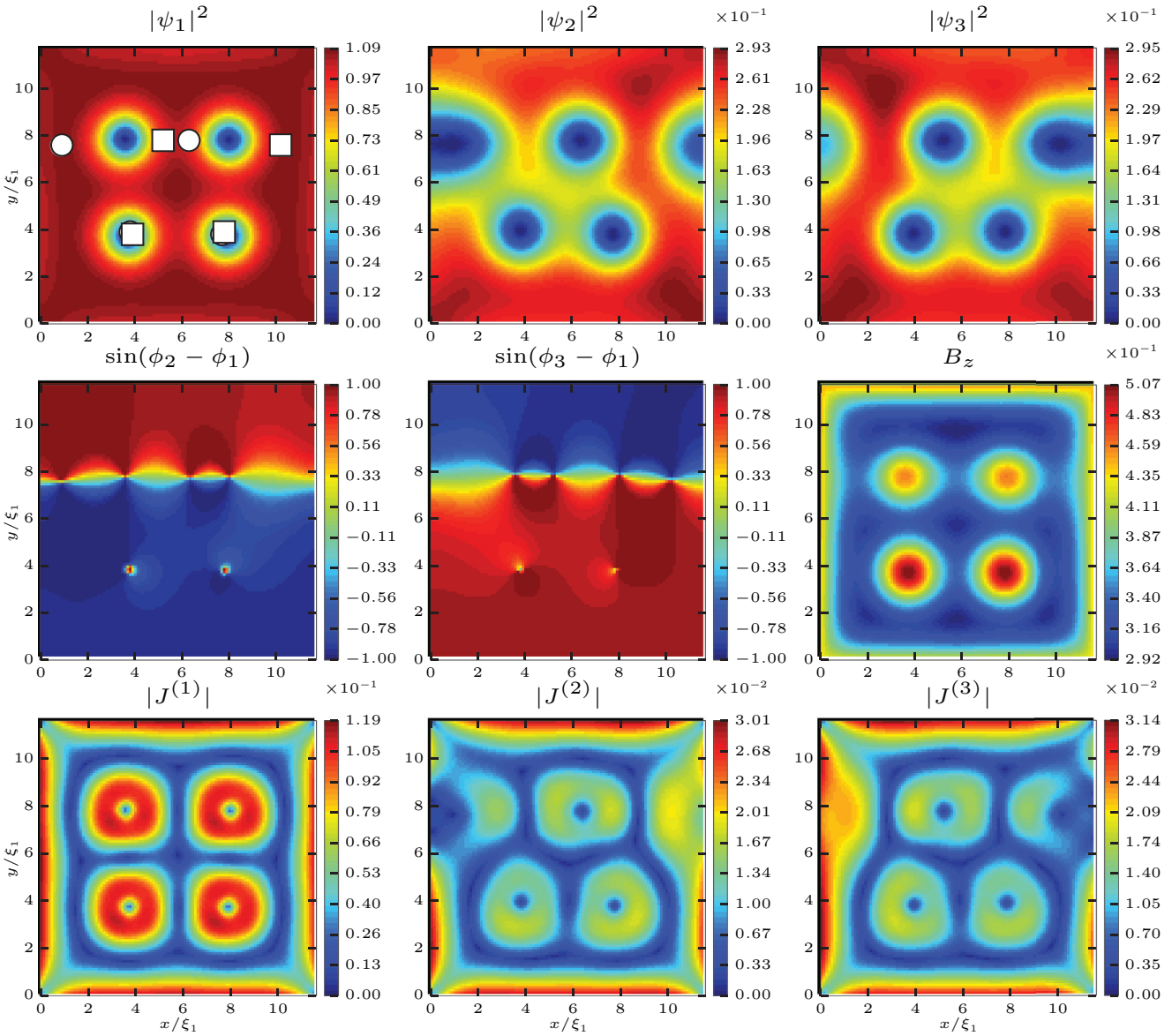


FIG. 10. (Color online) As Fig. 9, but for a state with a phase domain spanning across the sample.

Given an initial configuration $(\psi_i, \mathbf{A})$ we used either the quasi-Newton BFGS or conjugate gradient method, as implemented by the TAO[61] and PETSc[62] parallel numerical libraries, to find a local minimum of $\mathcal{F}$. Other parts of the program and support routines are an adaption of previous work done in Ref. 63. More details on the discretization can be found in Refs. 64 and 65.

## III. CLASSIFICATION OF VORTEX STATES

In this section we will classify in a comprehensive manner the many states found using the recipe described in the previous section. It is well known that even in single-band superconductors at a given external magnetic field there are multiple states possible, one ground state, and other metastable states–but all realizable in experiment. This can be accomplished for example by increasing the magnetic field until a new state with different vorticity emerges. If the magnetic field is subsequently decreased again, the new vortex state will not be destroyed immediately, thus one has found two different vortex states at a given magnetic field. As it turns out, the number of metastable states in three-band superconductors is far larger than in any single-band counterpart. Using the characteristic features of those states, we classify them in three main categories.

### A. Conventional vortex states

Vortex matter in mesoscopic single-band superconductors is well understood (see Refs. 26 and 34 and citing articles) and we will refer to similar states in three-band superconductors as "conventional vortex states." They comprise composite vortices, vortex configurations influenced by the geometry of the sample, and no phase difference between the band condensates.

Figure 2 shows the energy dependence of all the conventional vortex states found during the simulations as a

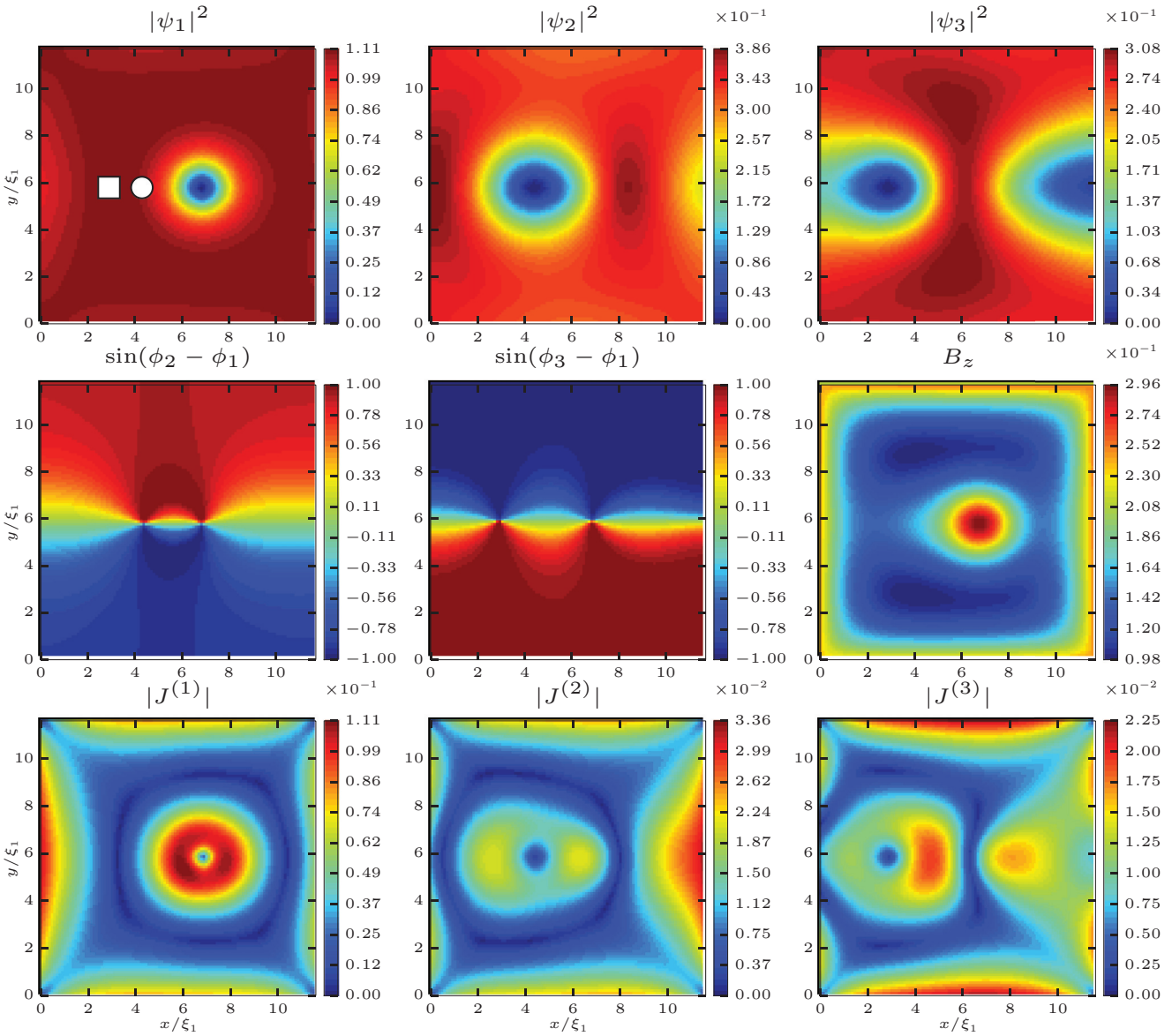


FIG. 11. (Color online) Chiral vortex state for $L = 1$ with notably broken spatial symmetry.

function of the externally applied magnetic field. Due to the Josephson coupling between the condensates, the second and third condensate become superconducting. Since there is no phase difference between the condensates, the passive bands have the same behavior as the active band.

We note that states for each vorticity have one corresponding curve, except for vorticity four, which has two. In Fig. 3(a) we show the lowest energy $L = 4$ state, while Fig. 3(b) shows the another stable state but with higher energy. The state in Fig. 3(b) is usually not found stable in single-band superconductors, which demonstrates subtly different interplay of (multicored) vortices with screening Meissner currents at the boundary of the multiband samples. In what follows, we show that differences are actually very pronounced.

### B. Chiral vortex states

It has already been shown in Refs. 49,51, and 52 that it is possible for three-band superconductors to have solutions with a phase difference between band condensates, which we refer to as chiral solutions. Figure 4 shows the energy of all found chiral vortex states, with the same vorticity in all bands. It is clear that the basic shape of Fig. 4 is the same as in Fig. 2, but more importantly the chiral states always have lower energy than the corresponding conventional state! Since for the same parameters Ref. 49 reported chiral states as higher energy ones, it is implied from our results that mesoscopic confinement enhances the chiral states and lowers their energy compared to the conventional states. Another important feature of chiral states is that they exhibit much larger metastability, i.e., more possibilities for a given vorticity. For example, we show in Fig. 5 the chiral counterparts of + and × configurations from Fig. 3. However, we also find different configurations for vorticity six for example, as shown in Fig. 6. These are not present among the conventional vortex states.

Another factor introducing excitations into the spectrum of chiral states with given vorticity are phase domain walls. These domain walls were identified as a source of split-core

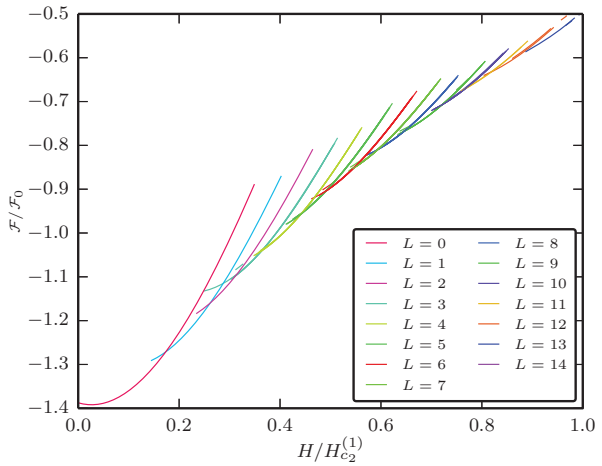


FIG. 12. (Color online) Energy curves of the chiral fractional states with one fractional vortex in the passive bands $(L_1, L_2, L_3) = (L, L+1, L+1)$, without domains in the phase difference between the band condensates.

vortex states in bulk three-component samples in Ref. 49, i.e., states in which vortex cores do not coincide in different band condensates. In Fig. 7 we show the split-core $L = 4$ state (cf. Fig. 5) where vortices in different bands minimize energy by separating along the internal phase domain wall (connecting the vortices, see the plot of phase difference in Fig. 7). However, this split-core vortex state has higher energy than both states of Fig. 5. Figure 8 shows the energy of all found chiral states with domain walls, i.e., with split-core vortices. We note three longer curves of vorticity four, six, and eight. These are states with internal domain walls as in Fig. 7. These states are more stable than the other states in Fig. 8, and are not present for every vorticity due to the competition of the vortex configuration with the sample geometry (i.e., its $C_4$ symmetry). These states are typically found in the simulations from the initial state shown in Fig. 1. States with different vorticity and an internal domain wall were not found.

However, besides the states with an internal domain wall, we found other states where the domain walls connect with the

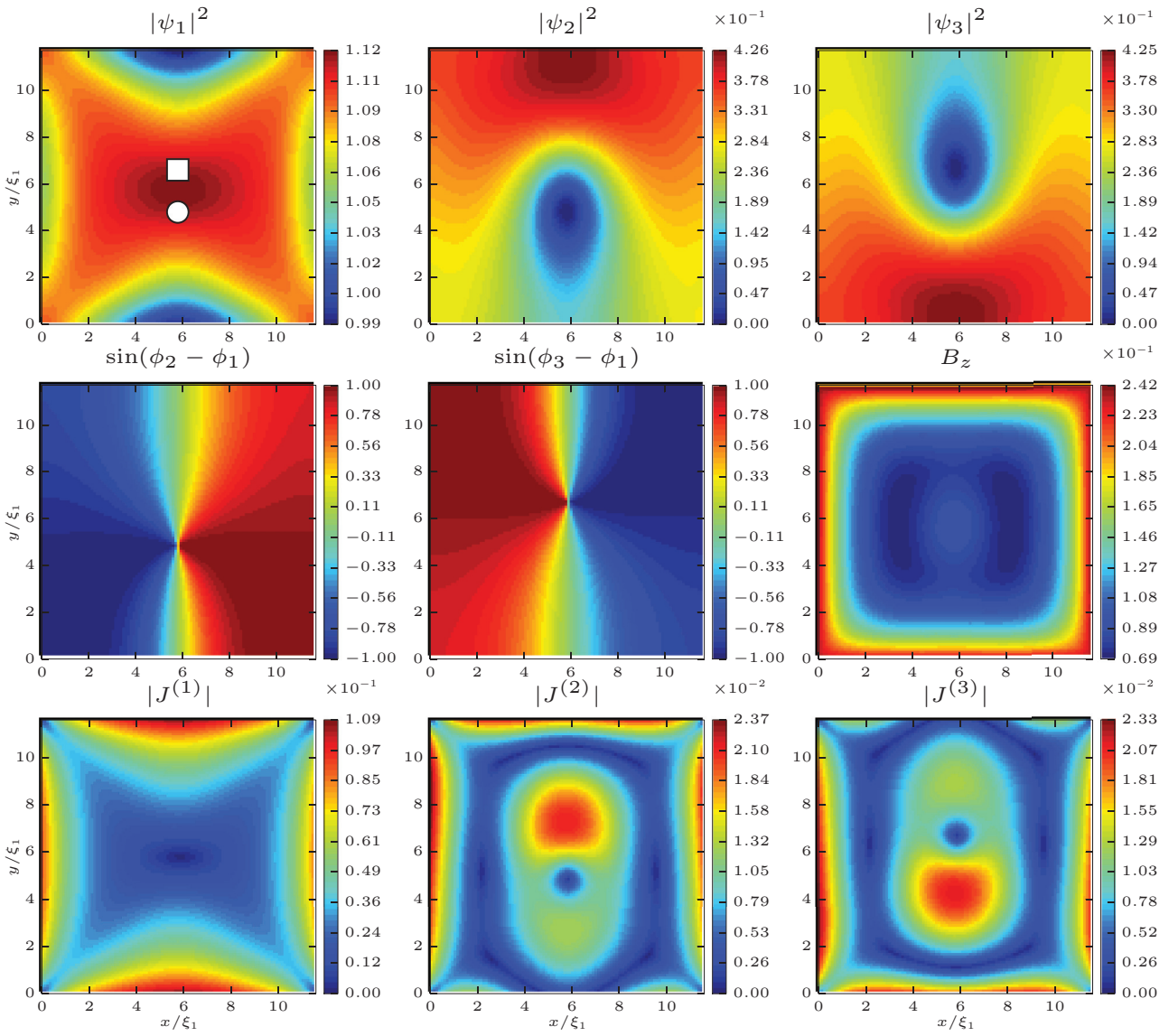


FIG. 13. (Color online) The chiral fractional vortex state (0,1,1).

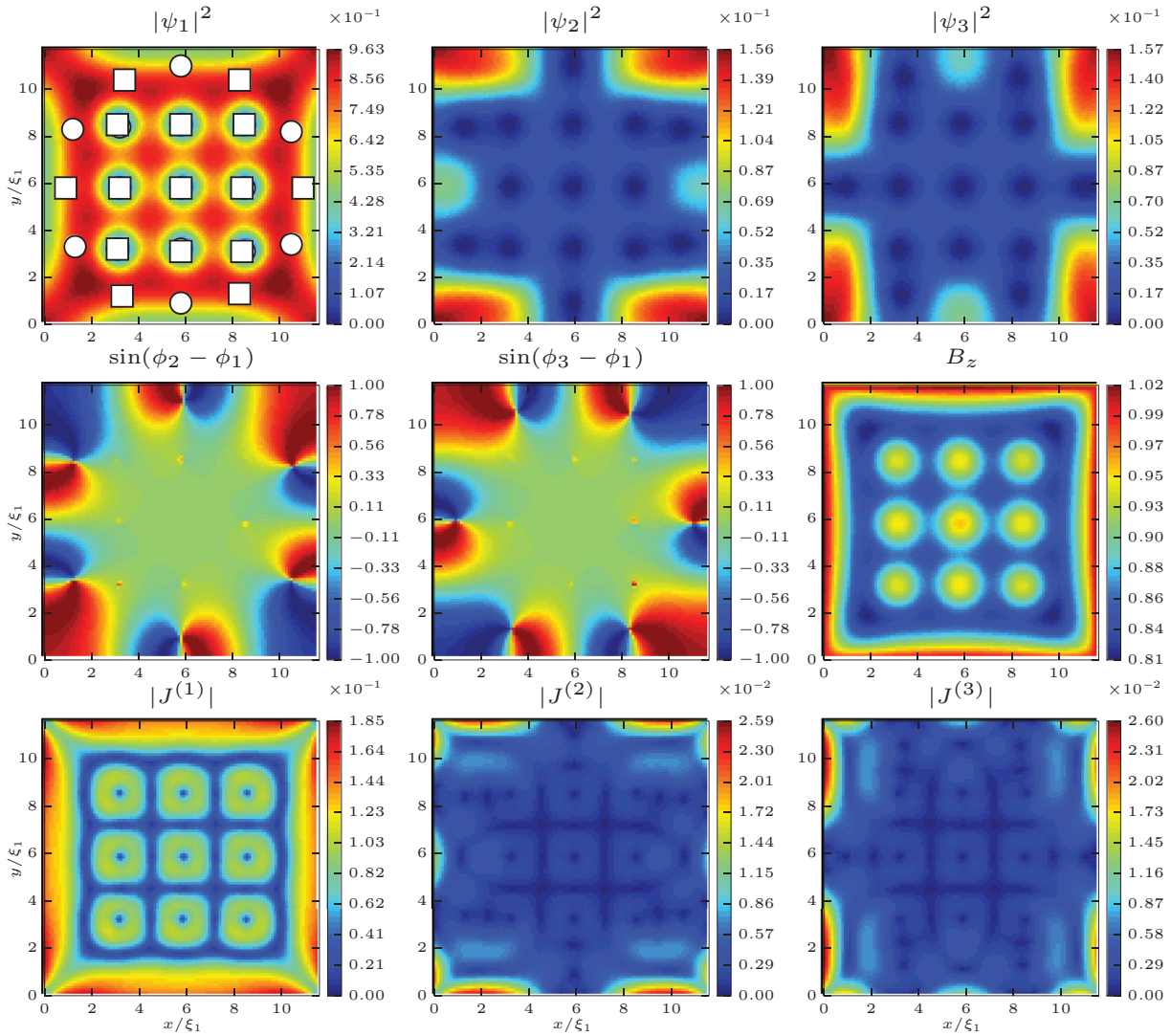


FIG. 14. (Color online) The chiral fractional vortex state (9,15,15), showing the case of six fractional vortices aside nine composite ones in the same sample.

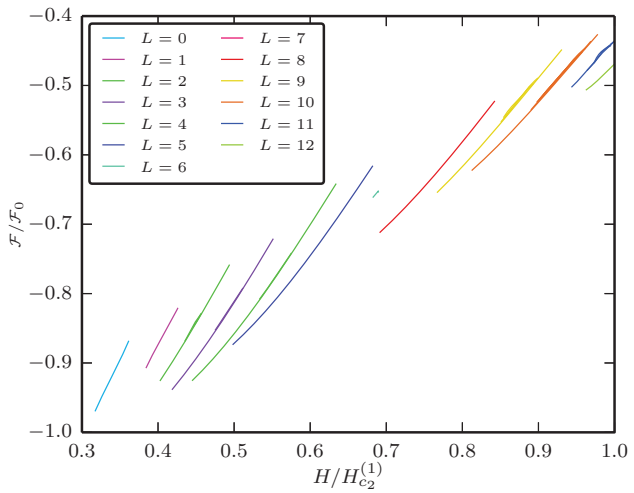


FIG. 15. (Color online) Energy of all found vortex states with four chiral fractional vortices in the passive bands $(L, L+4, L+4)$ regardless of the phase distribution.

sample boundary—which is a new mesoscopic effect. These states are very rich, and can form from an arbitrary initial condition, e.g., corresponding to a field-cooled experiment. To illustrate them, we show in Figs. 9 and 10 the found $L = 4$ chiral states with different geometry of the phase domain walls. In Fig. 9 the domain wall connects adjacent sides of the sample, whereas in Fig. 10 it spans across the sample. Such configurations of the domain walls strongly affect the observed vortex states, since the vortex configuration is now formed in a threefold competition between the sample geometry, number of vortices, and the geometry of the phase domain wall.

The presence of domain walls and favorable vortex splitting can therefore result in a very pronounced symmetry breaking, as shown in Fig. 11 for the $L = 1$ state. Due to the domain wall running across the sample, the vortices in different bands separate along that line, and the vortex present in the first condensate is not in the middle of the sample, which is directly observable in, e.g., scanning probe experiments. This configuration notably breaks the fourfold symmetry. By flipping the sign of the phase difference in both domains in

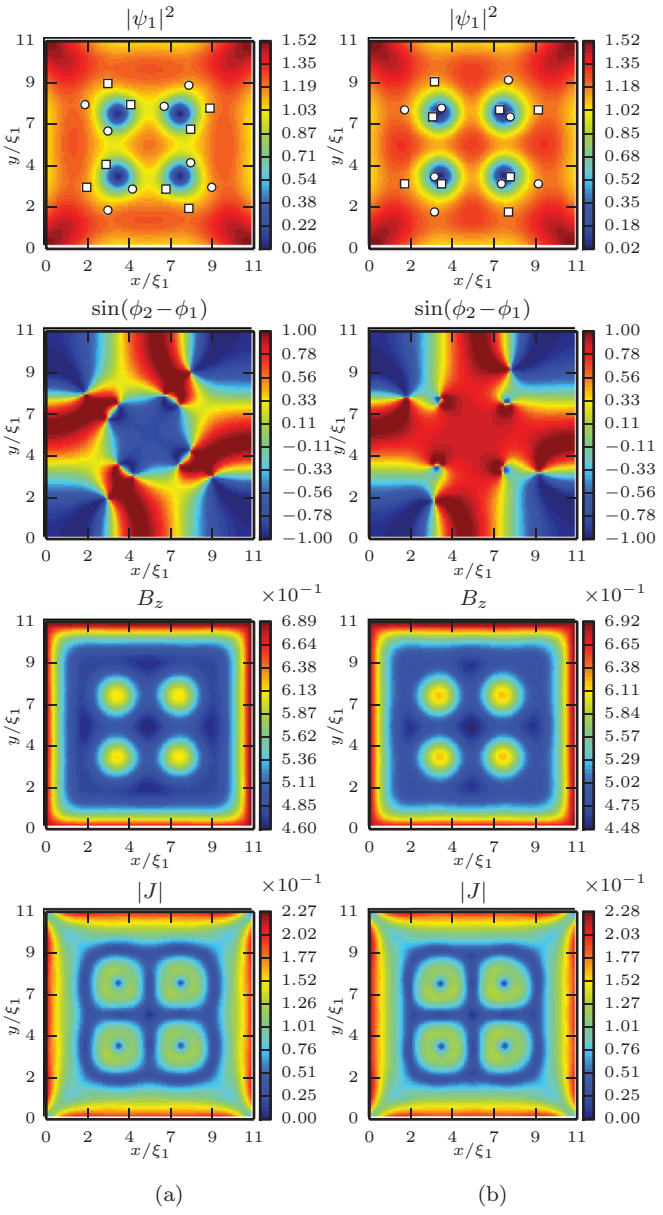


FIG. 16. (Color online) Vortex state (4,8,8), with four split-core vortices in all bands, and four chiral fractional vortices in the second and third bands. (a) A higher energy state, with an internal domain wall; (b) the state with no internal domain wall.

Fig. 11, the magnetic signature of the asymmetry will shift to the left instead of to the right.

Finally, we note that although states with a domain wall are more rich and intriguing, it is actually the chiral states without domain walls that are the ground states of this system at any given magnetic field. This suggests that latter states will be more likely found in experiments on chiral superconductors, but states with domain walls remain observable in, e.g., field-cooled experiments.

### C. Chiral fractional vortex states

In the previous sections we showed that (1) the system has solutions that behave as conventional vortex matter, where

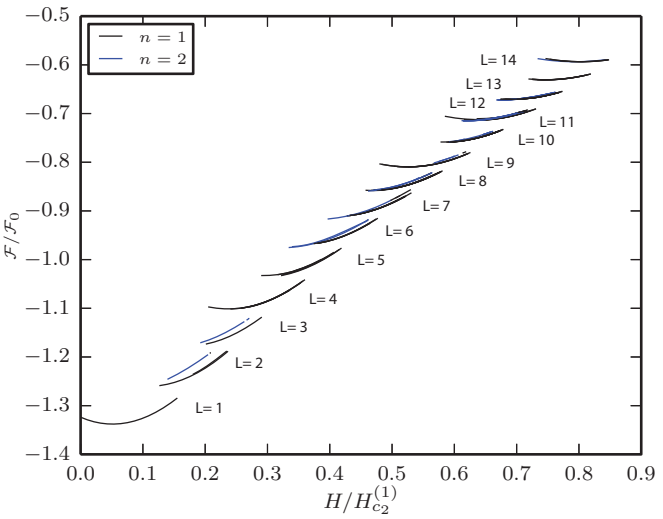


FIG. 17. (Color online) Energy of all found states with $n = 1,2$ fewer vortices in the passive condensates than in the active condensate, i.e., $(L+n,L,L)$ states, thus comprising $n$ fractional vortices only in the active band.

the passive bands show the same behavior as the active band, and (2) that there exist chiral solutions that actually have a lower free energy than the conventional vortex states in the frustrated system. Excited chiral states with phase domain walls were also possible. The latter actually stimulates vortex splitting along the domain walls, as discussed in Ref. 49. We introduced a term "split-core vortex" as a vortex that is noncomposite, i.e., the position of the vortex core in the three-band condensates is different. On the other hand, the difference in length scales between the condensates[18] should further affect the frustration, and according to Refs. 36 and 41 it could also lead to fractional vorticity, where a different number of vortices is found in different bands. The interplay of latter effects can therefore create numerous new equilibria in the system, which we will classify by the number of vortices in the passive bands compared to the active band for our choice of parameters. It should be noted however, that the usual fractional states in mesoscopic multiband superconductors, due to only competition of length scales (as discussed in Refs. 36 and 41), are not present in our system. In the absence of phase frustration, we have only found composite vortices for the chosen microscopic parameters (see Fig. 2). Therefore, the fractional vortices in the following sections are induced solely by phase frustration and time-reversal symmetry breaking, and are therefore called "chiral fractional vortices."

#### 1. *Larger vorticity in passive condensates*

We found a multitude of fractional states with more vortices in the passive bands compared to the active band. In Fig. 12 we show the energy spectrum of found states without a phase domain wall, and one additional fractional vortex in the passive bands. The observed behavior is fairly conventional, with exception of the less parabolic shape of the energy curves due to the fact that fractional vortices are easily expelled in a lowered magnetic field.

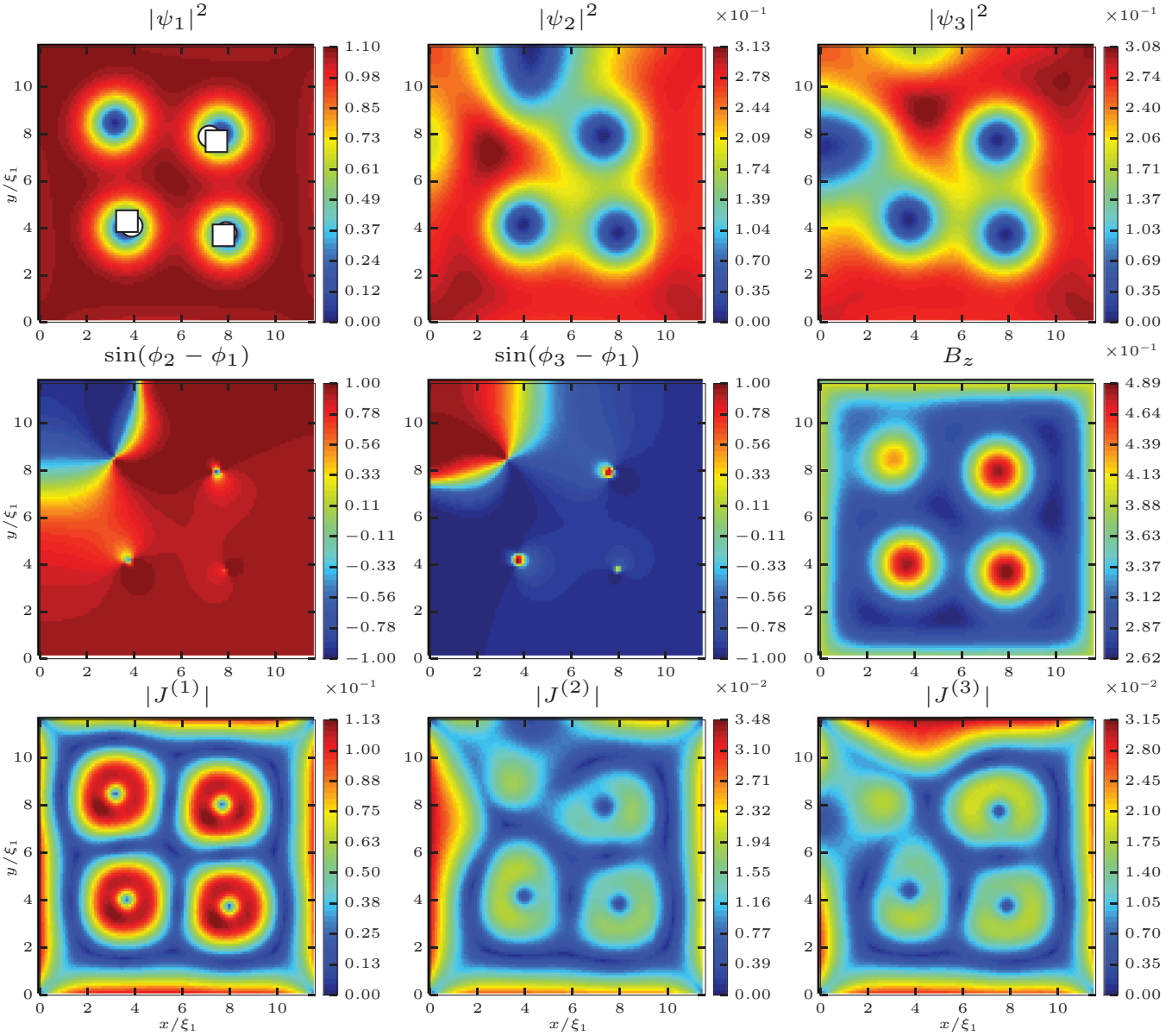


FIG. 18. (Color online) Example of a chiral state with four vortices in the active band, and three vortices in the passive bands. A phase domain wall runs through the single fractional vortex in the first band.

In Fig. 13 we show one example of a chiral fractional state from Fig. 12. We find that fractional vortices avoid each other due to time-reversal symmetry breaking, and in this particular example one vortex can be found in passive bands, whereas none is present in the active band. We label such a state as $(L_1, L_2, L_3) = (0,1,1)$. This state exhibits noninteger flux, spatial asymmetry of the condensates, and stray magnetic field whose profile does not directly show the presence of any vortices. The difference in vorticity between the bands can actually be larger than 1. In other words, it is possible to have more than one chiral fractional vortex in the system. In our simulations we found states with up to six (!) extra vortices in each passive band compared to the active one, an example of which is shown in Fig. 14 for the state (9,15,15).

Finally, in Fig. 15 we relax the condition on the phase, allow for the formation of the phase domain walls, and show the energy of all found states with four chiral fractional vortices, i.e., all possible states $(L, L+4, L+4)$. We see that some vorticities have two or more equilibria with a slightly different energy. We show an example of this metastability, found for the state (4,8,8), in Fig. 16. As was the case for the chiral vortex states with phase domain walls, the states with an internal domain wall always have higher energy compared to the state without the domain wall, but show more pronounced fractionalization, i.e., more separated vortex cores in the band condensates.

### 2. *Lower vorticity in passive condensates*

It is also possible that the passive condensates have less vortices than the active condensate, even though such states for our parameters have a narrower range of stability than those with more vortices in the passive bands considered in the previous subsection. Figure 17 shows the energy as a function

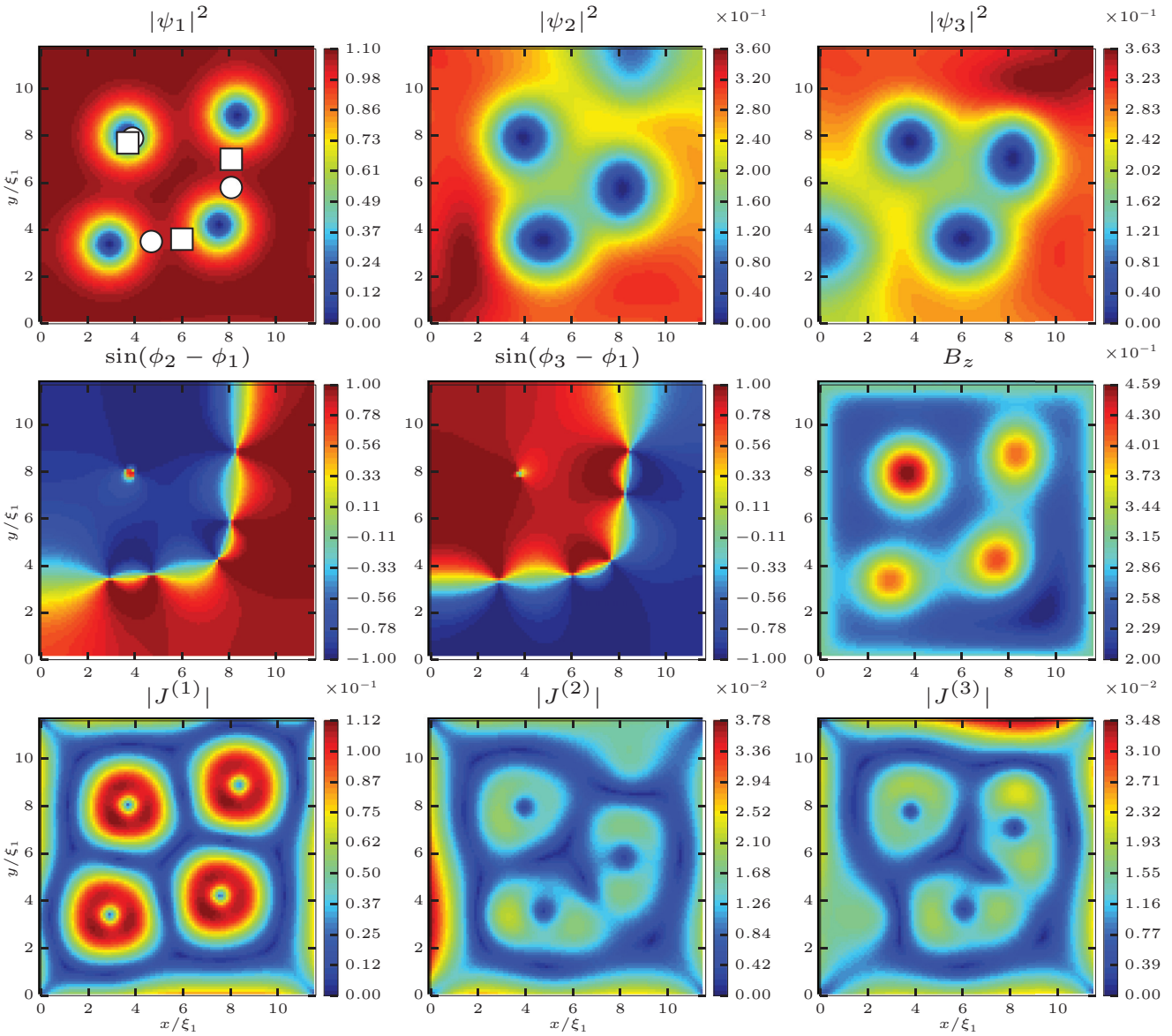


FIG. 19. (Color online) Another example of a state with same vorticity as in Fig. 18 This state has higher energy than the state shown in Fig. 18 due to the different symmetry and arrangement of vortices along the domain wall.

of the applied field for all the $(L+n,L,L)$ states, having $n = 1,2$ fewer vortices in the passive condensates. We note that for the chosen set of parameters there are only states found for either one or two extra vortices in the active band, indicating that fractional states with more vortices in the active band than in passive bands are indeed less favorable than the opposite, which is of course implied by the strong superconductivity in the active band.

In Fig. 18 we show an example of the (4,3,3) state with one extra vortex in the active condensate compared to the passive condensates ($n = 1$). The frustration is still visible in the loci of the vortex cores, although the fractional vortex is now only present in the active band. However, contrary to other examples of chiral fractional vortices (e.g., in Fig. 16) which were located in the passive bands, the fractional vortex in the active band leaves a clear magnetic signature in the spatial distribution of the magnetic field compared to the three composite vortices, observable by magnetic scanning microscopies (MFM, SHPM, etc.). It is peculiar that in this example we found a phase domain wall running exactly through the fractional vortex, which makes one wonder if other possibilities for the geometry of the domain wall are stable. In Fig. 19 we show one such possibility for the (4,3,3) state, exactly opposite to the case of Fig. 18. Now only one vortex is composite, and the domain wall runs through the remaining three vortices of the first band, and two in each other band, so that we seemingly have one composite and three fractional vortices in the magnetic response of the sample. In fact, there is only one truly fractional vortex on the domain wall, and other two are split-core vortices.

### 3. *Different vorticity in passive condensates*

The remaining class of chiral fractional states comprises ones where the number of vortices differs even between the two passive condensates. Figure 20 shows the energy dependence on the externally applied magnetic field of all fractional states

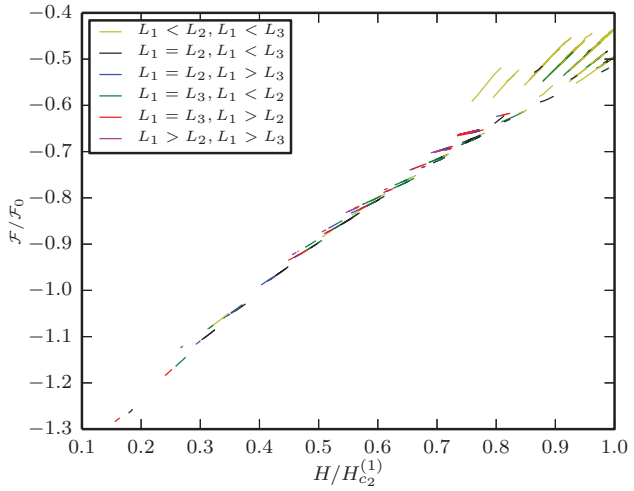


FIG. 20. (Color online) Energy of all found vortex states where the number of vortices in the second and third condensates are different.

with different vorticity in the passive condensates. An example of such state is shown in Fig. 21, for the (2,3,2) case, i.e., vorticity two in the first and third condensate, but vorticity three in the second. These states are essentially formed in the transition between the states discussed in the previous sections, where one chiral fractional vortex would leave the system before the accompanying fractions vanish as well, and are therefore much less stable than states shown in the previous sections. The exception are the states with larger vorticities in the passive bands, at higher applied fields; they are seemingly more stable, but that is of pure academic value since at such high fields and vorticities the passive bands are extremely depleted. It is worth noting here that the rarity of such states should be expected since the parameters of the passive bands are taken as identical. Should one investigate systems where all the bands have significantly different parameters, one would expect these states to become more common.

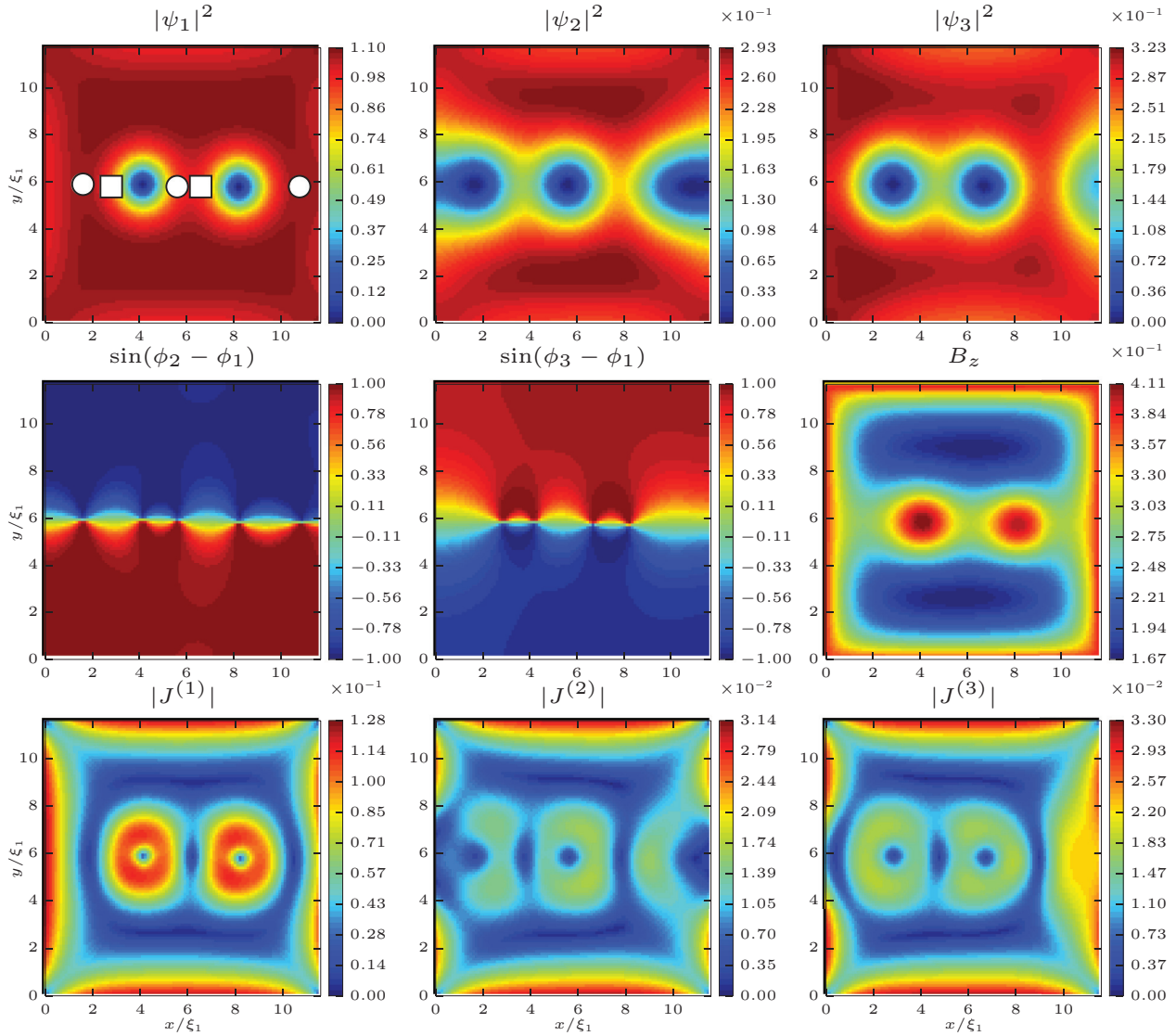


FIG. 21. (Color online) Vortex state with three vortices in the second condensate and two in the first and third condensate, with an internal phase domain wall and clear symmetry breaking.

## IV. CONCLUSION

In summary, we have studied in detail the intermediate state of a mesoscopic three-band superconductor, particularly with respect to possible phase frustration between the band condensates, using the three-component Ginzburg-Landau theory. We examined, described, and classified all the found vortex states in a mesoscopic three-band system (please see the interactive visualization tool of all states in the Supplementary Material[66]), some of which can be called *conventional*—with composite vortex cores in different bands (i.e., their cores are coaxial in three condensates), and no phase difference between the band condensates. As a first important result, we showed that the ground state of the system are the *chiral* states, in which phase difference is found between the band condensates, but vortices are still composite. This is an example of the chiral state as the ground state of the system at all magnetic fields, i.e., we find that the chiral state is enhanced by mesoscopic confinement. On the other hand, a state with noncomposite (called split-core) vortices was predicted as an excited state in bulk systems in Ref. 49 but for an existing internal phase domain wall on which vortices are located. Indeed, we have also found such *chiral split-core* vortex states in the mesoscopic system, where the presence of domain walls not only introduces split-core vortices, but can also lead to symmetry breaking, in more ways than one since the domain wall can have different configurations with respect to the topology of the sample boundaries. Finally, in a mesoscopic system, the different effect of confinement on different condensates can stabilize states with fractional flux, i.e., different vorticity in different bands, as is well known from the earlier two-band studies.[36,41] In the chiral case, vortex fractions in different bands avoid each other, and can differ in numbers, which opens the *chiral fractional* class of states—attainable only in mesoscopic systems. Here fractionalization follows from the domain walls of the phase difference between bands interacting with the sample boundaries and favoring vortex splitting, not from different length scales of the condensates. This plethora of distinct classes of vortex states makes a three-band mesoscopic system an excellent playground for further theoretical and experimental studies, where dynamics of condensates and (fractional) vortices, i.e., flux flow, creep, and phase slippage phenomena,[67] must be correspondingly rich. The same holds for Josephson junctions and SQUIDs made of multiband superconductors, or stacks of alternating multi- and single-band layers, where interplay of band-dependent electronic phases and different sorts of present vortex states plays a crucial role.

## ACKNOWLEDGMENTS

This work was supported by the Flemish Science Foundation (FWO). Critical remarks of Lucia Komendová are gratefully acknowledged.

[1] J. Nagamatsu, N. Nakagawa, T. Muranaka, Y. Zenitani, and J. Akimitsu, Nature (London) **410**, 63 (2001).
[2] H. J. Choi, D. Roundy, H. Sun, M. L. Cohen, and S. G. Louie, Phys. Rev. B **66**, 020513 (2002).
[3] F. Giubileo, D. Roditchev, W. Sacks, R. Lamy, D. X. Thanh, J. Klein, S. Miraglia, D. Fruchart, J. Marcus, and P. Monod, Phys. Rev. Lett. **87**, 177008 (2001).
[4] M. Iavarone, G. Karapetrov, A. E. Koshelev, W. K. Kwok, G. W. Crabtree, D. G. Hinks, W. N. Kang, E.-M. Choi, H.-J. Kim, and S. I. Lee, Phys. Rev. Lett. **89**, 187002 (2002).
[5] P. Szabó, P. Samuely, J. Kačmarčík, T. Klein, J. Marcus, D. Fruchart, S. Miraglia, C. Marcenat, and A. G. M. Jansen, Phys. Rev. Lett. **87**, 137005 (2001).
[6] H. Schmidt, J. F. Zasadzinski, K. E. Gray, and D. G. Hinks, Phys. Rev. Lett. **88**, 127002 (2002).
[7] F. Bouquet, R. A. Fisher, N. E. Phillips, D. G. Hinks, and J. D. Jorgensen, Phys. Rev. Lett. **87**, 047001 (2001).
[8] H. D. Yang, J.-Y. Lin, H. H. Li, F. H. Hsu, C. J. Liu, S.-C. Li, R.-C. Yu, and C.-Q. Jin, Phys. Rev. Lett. **87**, 167003 (2001).
[9] H. Suhl, B. T. Matthias, and L. R. Walker, Phys. Rev. Lett. **3**, 552 (1959).
[10] V. A. Moskalenko, Fiz. Met. Metalloved. **8**, 503 (1959).
[11] J. M. Blatt and C. J. Thompson, Phys. Rev. Lett. **10**, 332 (1963).
[12] A. Perali, A. Bianconi, A. Lanzara, and N. L. Saini, Solid State Commun. **41**, 181 (1996).
[13] D. Innocenti, N. Poccia, A. Ricci, A. Valletta, S. Caprara, A. Perali, and A. Bianconi, Phys. Rev. B **82**, 184528 (2010).
[14] L. Komendová, Y. Chen, A. A. Shanenko, M. V. Milošević, and F. M. Peeters, Phys. Rev. Lett. **108**, 207002 (2012).
[15] M. Silaev and E. Babaev, Phys. Rev. B **84**, 094515 (2011).
[16] E. Babaev and M. Speight, Phys. Rev. B **72**, 180502 (2005).
[17] A. Chaves, L. Komendová, M. V. Milošević, J. S. Andrade, G. A. Farias, and F. M. Peeters, Phys. Rev. B **83**, 214523 (2011).
[18] L. Komendová, M. V. Milošević, A. A. Shanenko, and F. M. Peeters, Phys. Rev. B **84**, 064522 (2011).
[19] A. A. Shanenko, M. V. Milošević, F. M. Peeters, and A. V. Vagov, Phys. Rev. Lett. **106**, 047005 (2011).
[20] S.-Z. Lin and X. Hu, Phys. Rev. B **84**, 214505 (2011).
[21] V. Moshchalkov, M. Menghini, T. Nishio, Q. H. Chen, A. V. Silhanek, V. H. Dao, L. F. Chibotaru, N. D. Zhigadlo, and J. Karpinski, Phys. Rev. Lett. **102**, 117001 (2009).
[22] T. Nishio, V. H. Dao, Q. Chen, L. F. Chibotaru, K. Kadowaki, and V. V. Moshchalkov, Phys. Rev. B **81**, 020506 (2010).
[23] Y. Tanaka, Phys. Rev. Lett. **88**, 017002 (2001).
[24] E. Babaev, Phys. Rev. Lett. **89**, 067001 (2002).
[25] E. Babaev, J. Jäykkä, and M. Speight, Phys. Rev. Lett. **103**, 237002 (2009).
[26] B. J. Baelus and F. M. Peeters, Phys. Rev. B **65**, 104515 (2002).
[27] V. A. Schweigert and F. M. Peeters, Phys. Rev. B **60**, 3084 (1999).
[28] W. Little and R. Parks, Phys. Rev. Lett. **9**, 9 (1962).
[29] V. Bruyndoncx, L. Van Look, M. Verschuere, and V. V. Moshchalkov, Phys. Rev. B **60**, 10468 (1999).
[30] A. Kanda, B. J. Baelus, F. M. Peeters, K. Kadowaki, and Y. Ootuka, Phys. Rev. Lett. **93**, 257002 (2004).
[31] M. V. Milošević, A. Kanda, S. Hatsumi, F. M. Peeters, and Y. Ootuka, Phys. Rev. Lett. **103**, 217003 (2009).
[32] B. Xu, M. V. Milošević, S.-H. Lin, F. M. Peeters, and B. Jankó, Phys. Rev. Lett. **107**, 057002 (2011).

[33]D. S. Golubović, M. V. Milošević, F. M. Peeters, and V. V. Moshchalkov, Phys. Rev. B **71**, 180502 (2005).
[34]V. A. Schweigert, F. M. Peeters, and P. S. Deo, Phys. Rev. Lett. **81**, 2783 (1998).
[35]T. Cren, L. Serrier-Garcia, F. Debontridder, and D. Roditchev, Phys. Rev. Lett. **107**, 097202 (2011).
[36]R. Geurts, M. V. Milošević, and F. M. Peeters, Phys. Rev. B **81**, 214514 (2010).
[37]P. J. Pereira, L. F. Chibotaru, and V. V. Moshchalkov, Phys. Rev. B **84**, 144504 (2011).
[38]M. A. Silaev, Phys. Rev. B **83**, 144519 (2011).
[39]J. C. Piña, C. C. de Souza Silva, and M. V. Milošević, Phys. Rev. B **86**, 024512 (2012).
[40]A. DeCol, V. B. Geshkenbein, and G. Blatter, Phys. Rev. Lett. **94**, 097001 (2005).
[41]L. F. Chibotaru and V. H. Dao, Phys. Rev. B **81**, 020502 (2010).
[42]L. F. Chibotaru, V. H. Dao, and A. Ceulemans, Europhys. Lett. **78**, 47001 (2007).
[43]Y. Kamihara, T. Watanabe, M. Hirano, and H. Hosono, J. Am. Chem. Soc. **130**, 3296 (2008).
[44]X. H. Chen, T. Wu, G. Wu, R. H. Liu, H. Chen, and D. F. Fang, Nature (London) **453**, 761 (2008).
[45]G. F. Chen, Z. Li, D. Wu, G. Li, W. Z. Hu, J. Dong, P. Zheng, J. L. Luo, and N. L. Wang, Phys. Rev. Lett. **100**, 247002 (2008).
[46]D. Lu, M. Yi, S.-K. Mo, J. Analytis, J.-H. Chu, A. S. Erickson, D. Singh, Z. Hussain, T. Geballe, I. Fisher *et al.*, Physica C **469**, 452 (2009).
[47]K. Kuroki, S. Onari, R. Arita, H. Usui, Y. Tanaka, H. Kontani, and H. Aoki, Phys. Rev. Lett. **101**, 087004 (2008).
[48]M. P. Allan, A. W. Rost, A. P. Mackenzie, Y. Xie, J. C. Davis, K. Kihou, C. H. Lee, A. Iyo, H. Eisaki, and T.-M. Chuang, Science **336**, 563 (2012).
[49]J. Garaud, J. Carlström, and E. Babaev, Phys. Rev. Lett **107**, 197001 (2011).
[50]J. Garaud, J. Carlström, E. Babaev, and M. Speight, Phys. Rev. B **87**, 014507 (2013).
[51]V. Stanev and Z. Tešanović, Phys. Rev. B **81**, 134522 (2010).
[52]N. V. Orlova, A. A. Shanenko, M. V. Milošević, F. M. Peeters, A. V. Vagov, and V. M. Axt, Phys. Rev. B **87**, 134510 (2013).
[53]V. Stanev, Phys. Rev. B **85**, 174520 (2012).
[54]X. Hu and Z. Wang, Phys. Rev. B **85**, 064516 (2012).
[55]P. Mele, K. Matsumoto, H. Nagayoshi, K. Fujita, Y. Yoshida, Y. Ichino, T. Kiss, A. Ichinose, M. Mukaida, B. Maiorov, F. F. Balakireva, S. A. Bailya, and L. Civalea, MRS Proc. **1434** (2013).
[56]M. J. Rice, H.-Y. Choi, and Y. R. Wang, Phys. Rev. B **44**, 10414 (1991).
[57]Q. H. Wang, C. Platt, Y. Yang, F. C. Zhang, W. Hanke, T. M. Rice, and R. Thomale, arXiv:1305.2317.
[58]D. Eom, S. Qin, M.-Y. Chou, and C. K. Shih, Phys. Rev. Lett. **96**, 027005 (2006).
[59]A. A. Shanenko, M. D. Croitoru, and F. M. Peeters, Phys. Rev. B **75**, 014519 (2007).
[60]A. A. Shanenko, N. V. Orlova, A. Vagov, M. V. Milošević, V. M. Axt, and F. M. Peeters, Europhys. Lett. **102**, 27003 (2013).
[61]S. Benson, L. C. McInnes, J. Moré, T. Munson, and J. Sarich, TAO User Manual (Revision 1.9), Tech. Rep. ANL/MCS-TM-242, Mathematics and Computer Science Division, Argonne National Laboratory (2007), http://www.mcs.anl.gov/tao.
[62]S. Balay, K. Buschelman, V. Eijkhout, W. D. Gropp, D. Kaushik, M. G. Knepley, L. C. McInnes, B. F. Smith, and H. Zhang, PETSc Users Manual, Tech. Rep. ANL-95/11, Revision 3.0.0, Argonne National Laboratory (2008).
[63]J. Jäykkä and J. M. Speight, Phys. Rev. D **84**, 125035 (2011).
[64]W. D. Gropp, H. G. Kaper, G. K. Leaf, D. M. Levine, M. Palumbo, and V. M. Vinokur, J. Comp. Physiol. **123**, 254 (1996).
[65]M. V. Milošević and R. Geurts, Physica C **470**, 791 (2010).
[66]See Supplemental Material at http://link.aps.org/supplemental/10.1103/PhysRevB.89.024512 for an interactive web page and associated data. The web page, `index.html`, initially consists of a $H$ vs $F$ plot of every simulation associated with the article. The user can click any of the plots to see a set of nine contour plots associated with that simulation: this plot has the same sub-panels as e.g. Fig. 1 in the main article. Clicking the plot again, removes the associated contour plots. Any number of contour plots can be displayed simultaneously. Please note that using the webpage requires javascript support and internet access (even if saved onto local computer).
[67]G. R. Berdiyorov, M. V. Milošević, and F. M. Peeters, Phys. Rev. B **79**, 184506 (2009).